ICAS-88-5.1.1

THREE DIMENSIONAL INVISCID FLOW CALCULATIONS IN TURBOMACHINERY COMPONENTS

Tony Arts

von Karman Institute for Fluid Dynamics
B - 1640 Rhode Saint Genèse - Belgium

ABSTRACT

The application of an Euler solver to the three dimensional, rotational, inviscid flow of a perfect gas in turbomachinery components is presented. The method is based on a time marching technique and a finite volume discretization procedure. The results on five different configurations are presented and compared either to experimental data or to other numerical procedures in order to demonstrate the generality and robustness of the method with respect to the type of geometry (axial/radial), of flow regime (subsonic/transonic) and of configuration (isolated blade row/full stage).

LIST OF SYMBOLS

CP_0 total pressure coefficient $\left[\frac{p_{01\ FS}-p_0}{p_{01\ FS}-p_2}\right]$

CP_s static pressure coefficient $\left[\frac{p_{01\ FS}-p}{p_{01\ FS}-p_2}\right]$

c	chord
e	total energy
M	Mach number
p	pressure
r,θ,z	cylindrical coordinates
S	coordinate along the blade
t	time
V	absolute velocity
W	relative velocity
α,β	blade-to-blade flow angles
γ	meridional flow angle
κ	isentropic coefficient
ρ	density
Ω	angular velocity

Subscripts, superscripts

ax	axial
cr	critical
is	isentropic
r,θ,z	cylindrical coordinates
0	total condition
1	upstream
2	downstream
3	downstream of rotor (stage calculation)

1. INTRODUCTION

During the past fifteen years, considerable improvement has been observed in the calculation of flows in turbomachinery. This progress is especially exemplified by the important development of time marching techniques combined with finite volume, finite difference or finite element approaches for the computation of internal inviscid and viscous flows. The Turbomachinery Department of the von Karman Institute has been involved for the last decade in the development of a set of programs allowing the computation of two and three dimensional, rotational, adiabatic inviscid flows of a perfect gas in turbomachinery components (isolated blade rows or stages), the flow regime being subsonic, transonic or supersonic.

The aim of the present contribution is to present a set of results obtained from the 3D approach. After a brief description of the method (a finite volume spatial discretization and time marching integration technique), the latter is successively applied to the calculation of flows in axial and radial turbomachinery components (isolated blade rows and stages, turbines and compressors). The aim of these different applications is to demonstrate the capabilities of this type of method to correctly predict overall characteristics of the flow as well as more detailed phenomena, e.g. secondary flows observed in a rotational flowfield. Whenever available, a comparison of the numerical results with measurements or results from other numerical procedures is provided.

2. LITERATURE SURVEY

Some of the first 3D methods to appear were singularity methods [1] for subsonic flows and methods of characteristics [2] for supersonic flows. However, one of the most popular approaches to solve 3D inviscid turbomachinery flows is still the time marching method. The first fully 3D inviscid solutions were reported by Denton [3]. Other methods were respectively proposed by Bosman & Highton [4], Brochet [5], Thompkins [6], Laskaris [7], Sarathy [8], Holmes & Tong [9], Koya & Kotake [10]. A detailed review of the development in numerical methods for turbomachinery flows was presented by McNally & Sockol [11]. As a matter of fact, the different contributions of this non exhaustive list differ principally by the author's choice for the spatial discretization technique or the numerical scheme applied during the time marching procedure. Most of these papers unfortunately show only applications to restricted configurations and give few examples to demonstrate the generality of the proposed procedure.

An investigation on the numerical simulation of 3D inviscid flows was also start-

ed in the Turbomachinery Department of the VKI. As a result, a set of programs was developed and successively applied to subsonic [12-15] and transonic [13,16] flows in single fixed blade rows, and to steady transonic flow in axial turbine stages [17].

3. CALCULATION METHOD

3.1 Flow domain

The flow domain is made up of one blade passage and extends upstream and downstream, approximately in the flow direction, over a distance of the order of a characteristic dimension (chord, pitch, ...) of the blade row. It is discretized using three families of surfaces. The streamwise surfaces (surfaces of revolution) are eventually variably spaced along the height of the blade and are limited by the hub and tip endwalls. The bladewise surfaces are evenly spaced along the circumferential direction and are limited by the suction side of one blade and the pressure side of the adjacent one. The spanwise surfaces (surfaces of revolution) are variably spaced along the meridional direction between the inlet, leading edge, trailing edge and outlet planes. The choice of the control volume is based on an analysis of consistency and order of accuracy [18,19]. It is made up of two almost regular polyhedra defined by the three above mentioned families of surfaces. The corresponding position of the nodes in which the flow characteristics are computed is shown in figure 1.

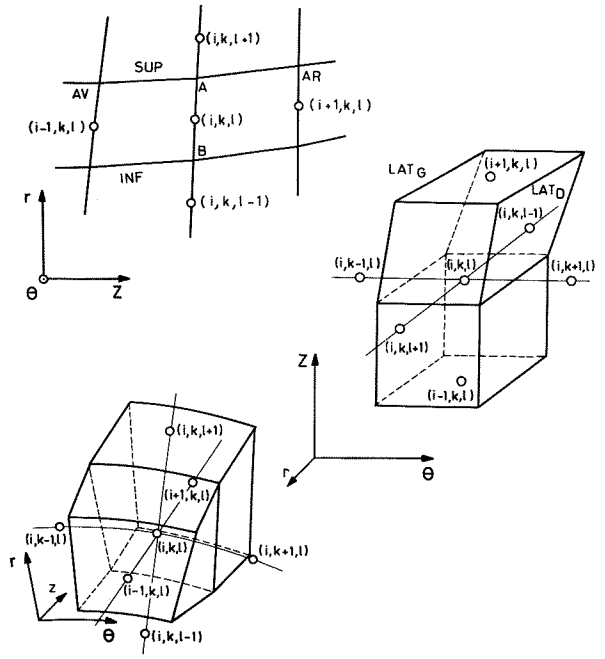

Fig. 1 - Computational molecule

3.2 Equations

The partial differential system to solve is the 3D Euler system of equations, written in a time dependent form and expressed in a cylindrical system of coordinates (r,θ,z). The latter is fixed to the blade row which eventually rotates at a constant angular velocity Ω around the z- axis, coinciding with the machine axis. The equations are non-dimensionalized by a characteristic length and by the inlet total thermodynamic conditions and are written as follows :

$$\frac{\partial \vec{\sigma}}{\partial t} + \frac{1}{r}\frac{\partial}{\partial r}\left[r\vec{f}(\vec{\sigma})\right] + \frac{1}{r}\frac{\partial}{\partial \theta}\left[\vec{g}(\vec{\sigma})\right] + \frac{\partial}{\partial z}\left[\vec{h}(\vec{\sigma})\right] + \vec{b}(\vec{\sigma}) = 0 \qquad (1)$$

$$\vec{\sigma} = \begin{bmatrix} \rho \\ \rho W_r \\ \rho W_\theta \\ \rho W_z \\ \rho e \end{bmatrix}$$

$$\vec{b}(\vec{\sigma}) = \begin{bmatrix} 0 \\ -\rho W_\theta^2/r \quad -p/r \quad -\rho r\Omega^2 \quad -2\rho\Omega W_\theta \\ \rho W_r W_\theta/r \quad +2\rho\Omega W_r \\ 0 \\ 0 \end{bmatrix}$$

$$\vec{f}(\vec{\sigma}) = \begin{bmatrix} \rho W_r \\ \rho W_r^2 + p \\ \rho W_r W_\theta \\ \rho W_r W_z \\ \rho W_r (e + \frac{p}{\rho}) \end{bmatrix} \qquad \vec{g}(\vec{\sigma}) = \begin{bmatrix} \rho W_\theta \\ \rho W_r W_\theta \\ \rho W_\theta^2 + p \\ \rho W_\theta W_z \\ \rho W_\theta (e + \frac{p}{\rho}) \end{bmatrix}$$

$$\vec{h}(\vec{\sigma}) = \begin{bmatrix} \rho W_z \\ \rho W_r W_z \\ \rho W_\theta W_z \\ \rho W_z^2 + p \\ \rho W_z (e + \frac{p}{\rho}) \end{bmatrix}$$

The closure relation is provided by the perfect gas law :

$$p = (\kappa - 1)\left[\rho e - \frac{1}{2}\rho(W_r^2 + W_\theta^2 + W_z^2) + \frac{1}{2}\rho\Omega^2 r^2\right] \qquad (2)$$

System (1) is expressed in a quasi conservative form; it can also be shown that it is hyperbolic with respect to time for all flow regimes: subsonic and supersonic.

3.3 Numerical scheme

System (1) is solved by means of a time marching technique and a finite volume discretization procedure, i.e., integrated with respect to time and volume. The time derivative is discretized by means of the corrected viscosity scheme, introduced by McDonald [20,21]. This numerical scheme has been used intensively for 1D [22,23], 2D [22,24,25] and 3D [12-18] flow calculations

and has shown good properties of convergence, stability and accuracy. The spatial integration is applied onto the polyhedron defined in §3.1. The details of the technique are described in [12,18].

The primary reason for the choice of this numerical scheme was not to propose an improved method showing much better accuracy or much shorter calculation time than existing ones. The selection of this relatively old but well-documented and robust technique was dictated by the objective to design a program that could be used as a "black box", without any tuning by non specialists for practical industrial applications on different types of geometries.

3.4 Boundary conditions

In order to have a mathematically well posed problem the partial differential system of equations(1) must be completed by a set of conditions along the boundaries of the computational domain. Classical periodicity and impermeability conditions are enforced respectively along the periodical and blade, hub and tip boundaries. In the inlet plane, the given conditions are the meridional and blade-to-blade (or swirl) angles and the absolute pressure and temperature. The spanwise distribution of these quantites is defined by the user whereas their pitchwise distribution is assumed to be uniform. In the outlet plane, the static pressure, uniform in the pitchwise direction, is specified at a given position. The spanwise distribution is obtained from a generalized radial (for axial geometries), axial (for radial geometries) or mixed equilibrium condition; the latter is obtained from a suitable combination of the radial and axial momentum equations.

3.5 Convergence criteria

The convergence of the calculation is checked using the following criteria :
-the maximum relative change in density over one time step is reduced to a value of 10^{-5}
-the maximum difference between the mass flow through a spanwise discretization surface and the mean mass flow is reduced below 1% for axial configurations and below 5% for radial configurations. The difference between inlet and outlet mass flow is, however, at least one order of magnitude smaller;
-the pitchwise mass averaged outlet flow angle in the blade-to-blade plane at a reference radius is maintained at a constant value, within ±0.1°.

4. NUMERICAL APPLICATIONS

A number of practical applications of the proposed method will be described in this section. The results obtained for these different test cases will, however, not be presented in detail : only some typical features will be pointed out. Complementary information for some of these configurations are available in former contributions.

4.1 Ultimate stator of a large steam turbine

The choice of this type of geometry was dictated by two main reasons : existence of strong 3D effects because of the important geometrical variations and definite presence of transonic flow. This cascade was proposed as a test case during one of the von Karman Institute Lecture Series [26]. Measurements are unfortunately not available but comparisons with 2D calculation results will be presented.

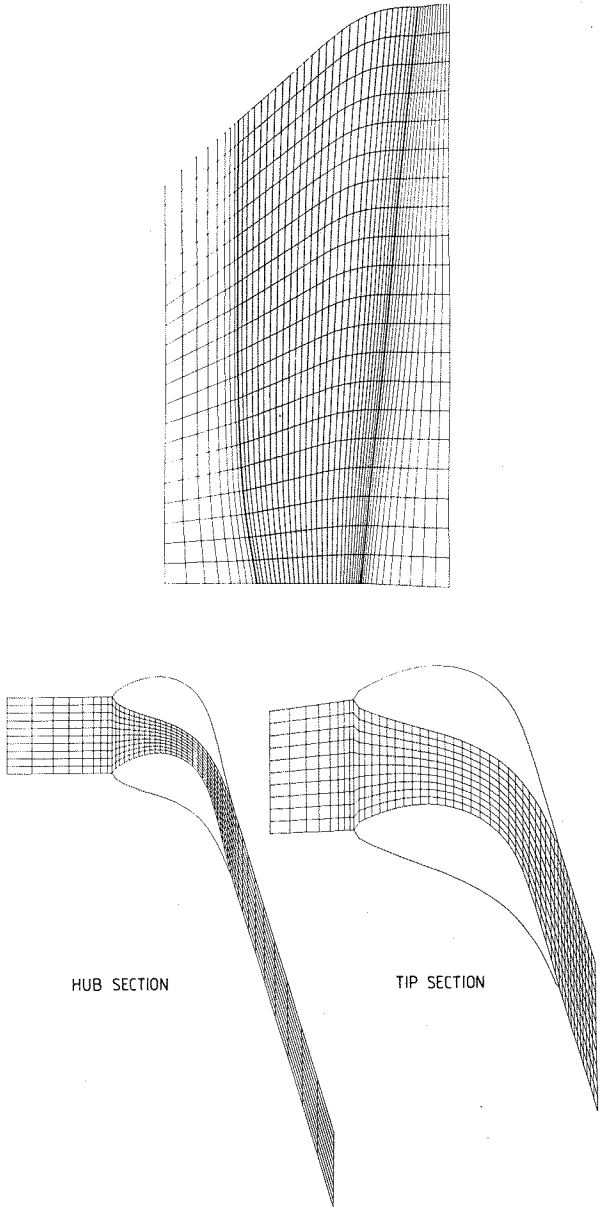

Fig. 2-Ultimate stator of a large steam turbine : computational domain

The computational domain (Fig. 2) consists of 49 spanwise surfaces (29 of them between leading and trailing edge), 21 streamwise surfaces (including hub and tip endwalls) and 11 bladewise surfaces (including suction and pressure surfaces). The inlet conditions are axial flow (in the blade-to-blade plane) and constant total pressure and total temperature profiles. The static pressure was imposed at the hub downstream of the blade row, corresponding to an isentropic Mach number of 1.436. An isentropic coefficient κ equal to 1.3 was used, according to the principle of a frozen speed of sound [27]. The computed spanwise distributions of Mach number and blade-to-blade flow angle in the exit plane are presented in figure 3. The supersonic angle deviation is clearly observed in the hub region. The blade Mach number distributions at hub, midspan and tip are plotted in figure 4(a,b,c). A nearly constant acceleration with small trailing edge shocks is observed in the hub region whereas decelerations are observed in the tip region.

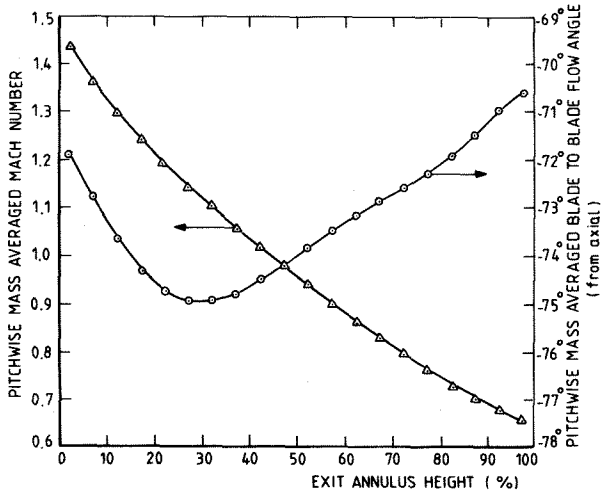

Fig. 3 - Ultimate stator for a large steam turbine : downstream conditions

The comparison with results obtained from 2D calculations is presented in the same figures. A classical method [24] was used; the calculations were performed at a constant radius, equal, for each 2D section, to the mean value between the leading edge and trailing edge radii of the corresponding 3D quasi-streamline, and without streamtube thickness variation. The 3D effects are clearly visible, especially in the tip region. It was also shown [16] that a quasi 3D approach, taking radius and streamtube thickness variations into account, does not provide a better prediction of the 3D effects.

Examples of typical 3D effects of the flow are shown for three different spanwise discretization surfaces (z/c_{ax}=0.630, 0.970, and 1.064) in figures 5 (iso-Mach number contours) and 6 (iso-meridional flow angle contours).

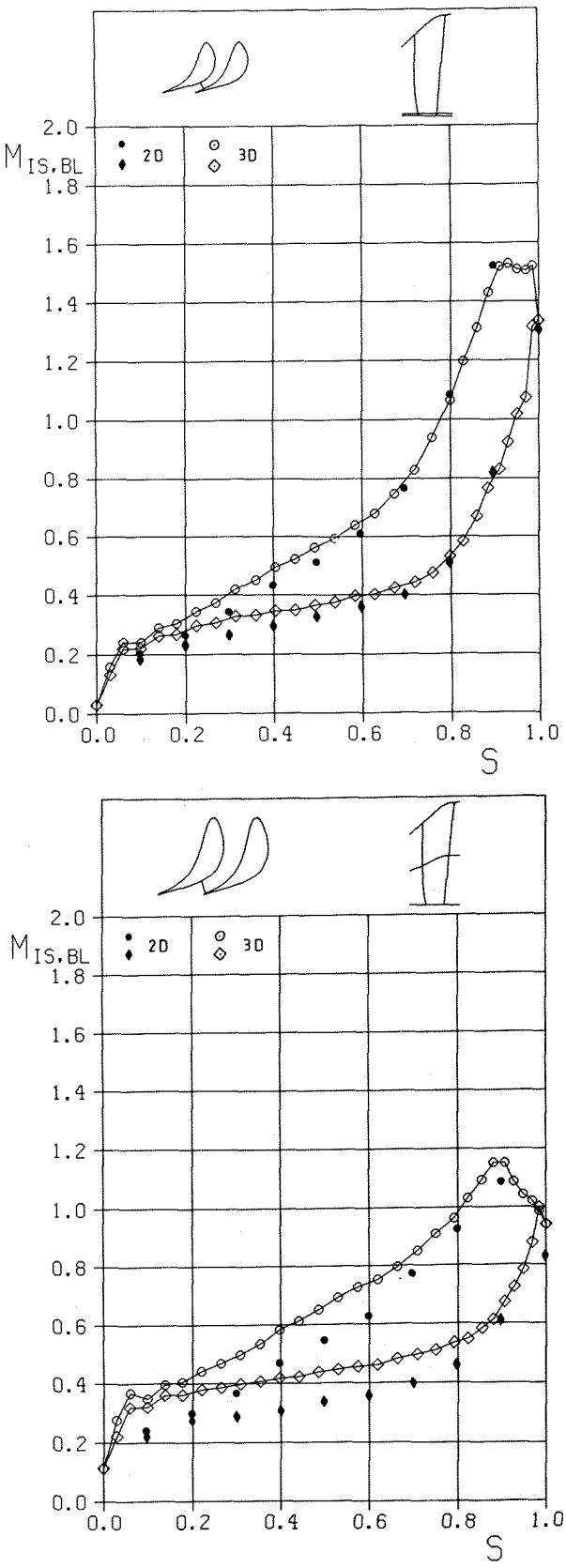

Fig. 4-Ultimate stator of a large steam turbine : blade velocity distributions

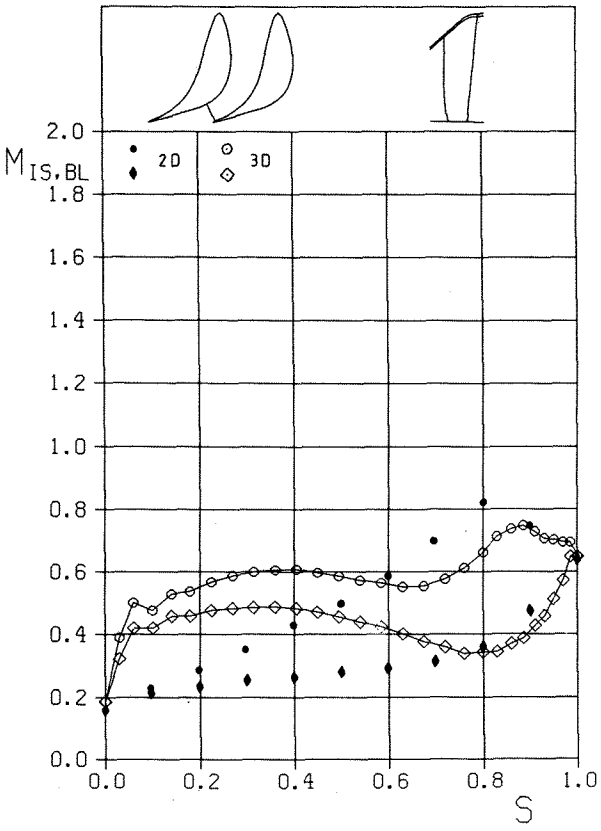

Fig. 4 (cont'd)

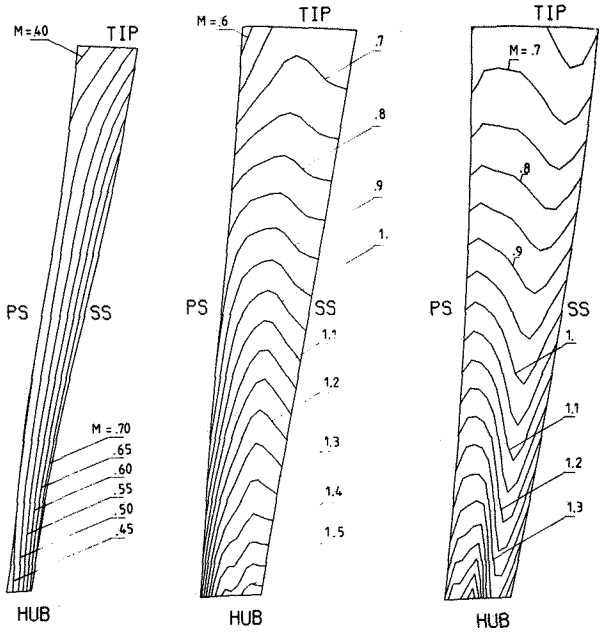

Fig. 5-Ultimate stator of a large steam turbine : iso Mach lines

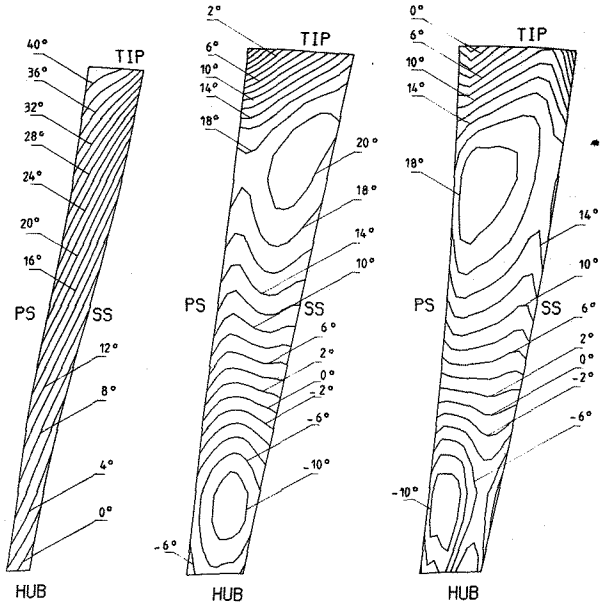

Fig. 6-Ultimate stator of a large steam turbine : iso γ angle lines

4.2 Low aspect ratio turbine nozzle guide vane with meridional contraction

The particular application intends to look at the capabilities of the code to correctly predict some of the main secondary flows (e.g. vortices and angle deviations) observed in an axial nozzle guide vane. The results presented in this section support the statement that the horseshoe and passage vortices are inviscid phenomena caused by the existence of vorticity in the incoming flow, although the origin of this vorticity is the viscous endwall boundary layer.

The program was applied to the calculation of the flow in the low aspect ratio (0.6), high turning (66°) annular turbine nozzle guide vane with meridional tip endwall contouring experimentally investigated under incompressible flow conditions at the von Karman Institute [28]. The flow was observed to be highly 3D due to the presence of the meridional endwall contraction and to the existence of secondary flows. Geometry, as well as measurement conditions and results are completely documented in [28]. The computational domain (Fig. 7) consists of 65 spanwise surfaces (41 of them between leading and trailing edge), 31 streamwise surfaces (including hub and tip endwalls) and 21 bladewise surfaces (including suction and pressure side). The inlet conditions are purely axial flow, a constant total temperature distribution and a spanwise total pressure profile determined from the measured upstream boundary layer profile (Fig. 8). Downstream of the blade row, the static pressure was imposed at the hub, corresponding to an isentropic Mach number value of 0.3. The measured and computed exit conditions are compared at z/c_{ax}=1.3 under the form of a pitchwise mass averaged static pressure coefficient (Fig. 9).

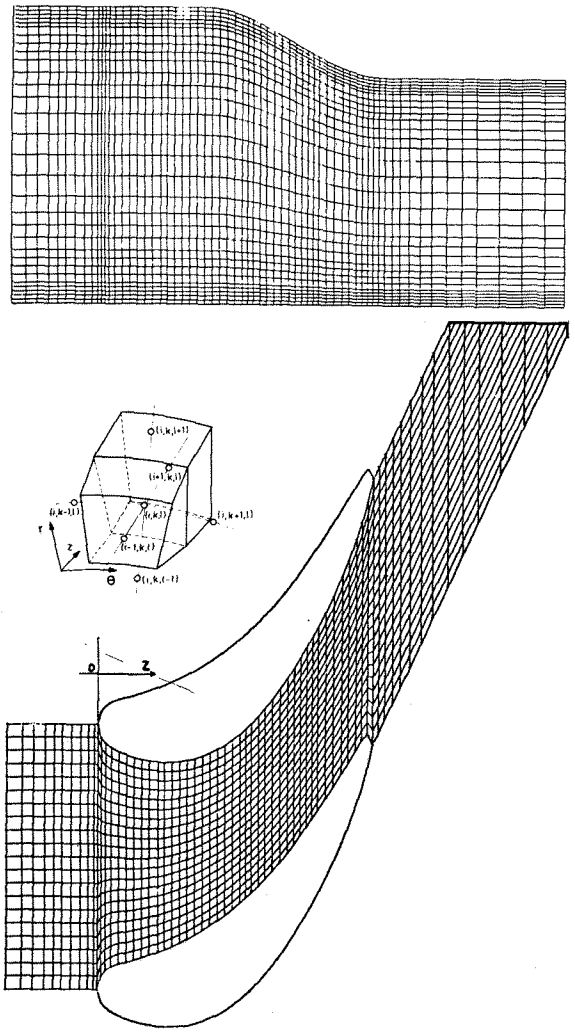

Fig. 7-Low aspect ratio turbine nozzle guide vane : computational domain

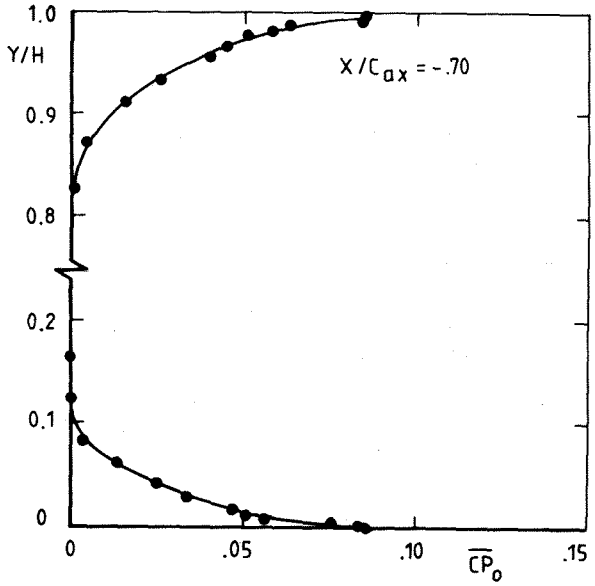

Fig. 8-Low aspect ratio turbine nozzle guide vane : inlet total pressure profile

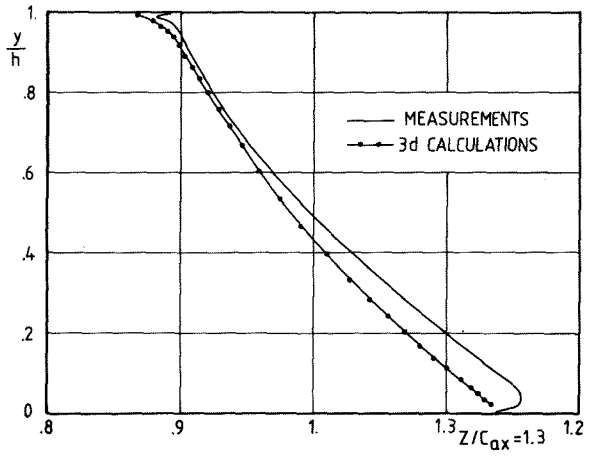

Fig. 9-Low aspect ratio turbine nozzle guide vane : downstream static pressure distribution

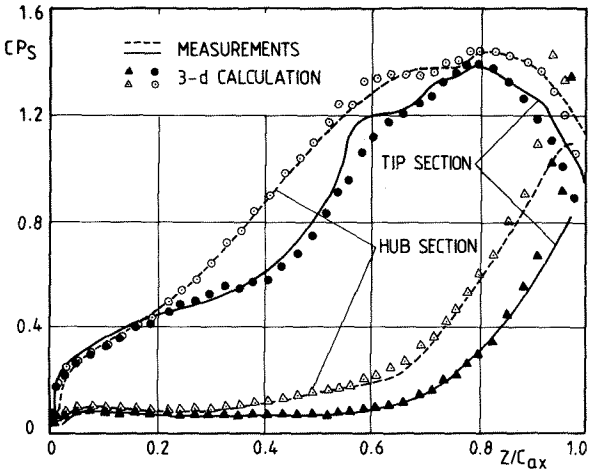

Fig. 10-Low aspect ratio turbine nozzle guide vane : blade velocity distributions

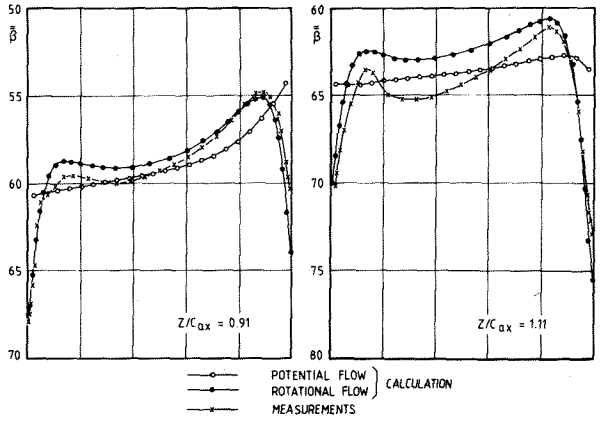

Fig. 11-Low aspect ratio turbine nozzle guide vane : blade-to-blade angle distributions

The measured and computed blade velocity distributions at hub and tip are presented in figure 10. As expected from endwall contouring, an important unloading of the front part of the vane is observed in the tip region. The calculated spanwise distributions of the pitchwise mass averaged blade-to-blade flow angle are compared with the measurements and with results obtained from a potential flow calculation in figure 11. The potential results were obtained from the same program but enforcing a uniform upstream total pressure profile. Inside the passage (z/c_{ax}=0.91), the under- and overturning are quite well predicted. More downstream, however, (z/c_{ax}=1.11) the influence of a purely inviscid downstream periodicity condition affects the prediction of the underturning. The velocity vectors (constructed from the axial and radial components) of the flow approaching the leading edge along a quasi stagnation line are shown in figure 12. The horseshoe vortex onset is clearly seen, and the existence of reverse flow is observed. Secondary velocities in three spanwise discretization planes are shown in figure 13. These secondary velocities were obtained from the difference between the rotational and potential calculations. At z/c_{ax}=0.01, the two legs of the horseshoe vortex appear clearly. At z/c_{ax}=0.42, some trace of the suction side leg is still present in the suction side/endwall corner while the pressure side leg is fully developed into the passage vortex. At z/c_{ax} = 0.91, only the passage vortex is still observed.

4.3 Single stage axial turbine

The flow through two successive blade rows in relative motion is basically unsteady. For a 2D geometry, some authors (e.g. [29,30]) have tried to model this situation by assuming a periodic behavior of all flow unknowns. Depending on the relative number of vanes and blades, the rotor sees periodically the same entrance flow pattern. However, due to substantial CPU times and large memory requirements, this approach cannot reasonably be extended to 3D configurations.

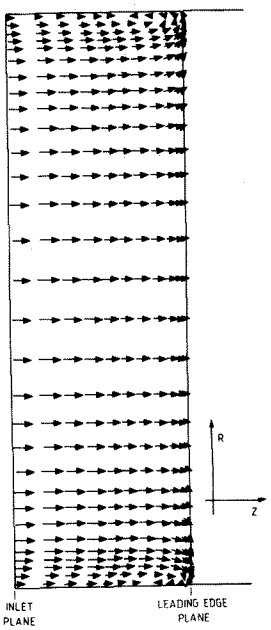

Fig. 12-Low aspect ratio turbine nozzle guide vane : horseshoe vortex

The alternative approach [31,32,17,10] is to make the assumption of a time-averaged flow. Upstream of each blade row, along the span, the tangential variation of all flow properties is set to zero, providing a mean or steady interaction between fixed and rotating blade rows. Two interconnected 3D blade row calculations are performed simultaneously : one in the stator and one in the rotor. The inter-row boundary conditions are repeatedly adapted until stabilization and correspondence of mass flow in both blade rows. The details of the procedure are given in [17,18].

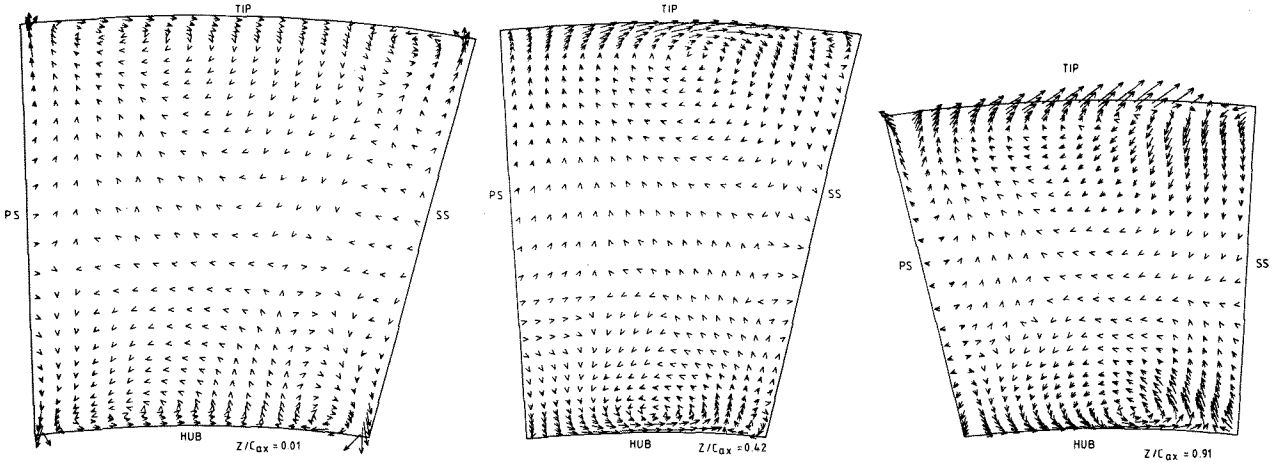

Fig. 13-Low aspect ratio turbine nozzle guide vane : secondary velocities

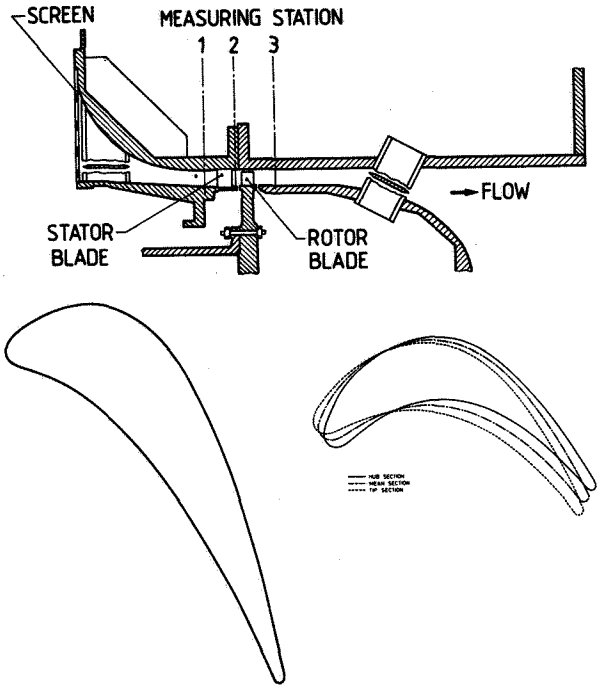

Fig. 14-Single stage axial turbine : meridional and blade-to-blade geometry

Calculations were performed on a single stage turbine with high work output tested at NASA [33]. The meridional and blade-to-blade geometry of the stage is shown in figure 14. Both blade rows were discretized by means of 49 spanwise surfaces (29 of them between leading and trailinbg edge), 11 bladewise surfaces (including suction and pressure surfaces) and 11 streamwise surfaces (including hub and tip). The inlet conditions to the stage were purely axial flow and uniform total pressure and total temperature profiles. The overall static to total pressure ratio of the stage was fixed at the hub to a value of 0.225, corresponding to the nominal regime. The corrected rotational speed was 8081 rev/min and the isentropic coefficient value was fixed at 1.4.

The measured mass flow was 3.856kg/s and a value of 3.95 kg/s was obtained from the calculation. The 2.4% overestimation is principally due to the fact that no losses were considered in this approach. The following table compares the measured and computed velocity triangles at midspan.

	Measurements	Calculations
V_2 (m/s)	325.6	318.40
α_2 (°)	72.25	72.72
W_2 (m/s)	149.1	145.7
β_2 (°)	48.26	48.02
V_3 (m/s)	197.8	193.6
α_3 (°)	-22.60	-18.9
W_3 (m/s)	330.0	319.3
β_3 (°)	-56.40	-54.98

The blade velocity distributions were only measured along the stator. The comparison with the calculated ones is shown in figure 15. The comparison is fairly good in the hub and midspan regions whereas some slight discrepancies are observed in the rear part of the suction side in the tip region. More detailed results are presented in [17].

4.4 Radial inflow turbine rotor

The present program was basically developed for axial flow turbines, especially with respect to consistency and accuracy requirements for the definition of the control volume and the choice of the spatial discretization procedure. A check of the ability of the code to also correctly deal with radial component flows was therefore absolutely necessary. A radial inflow turbine is considered in the present section. The rotor passages are highly 3D and have low aspect ratios compared with axial turbines. Moreover, these geometries, which turn the flow through 90° deflection in the meridional plane while simultaneously turning the flow in the blade-to-blade plane, naturally induce large 3D effects.

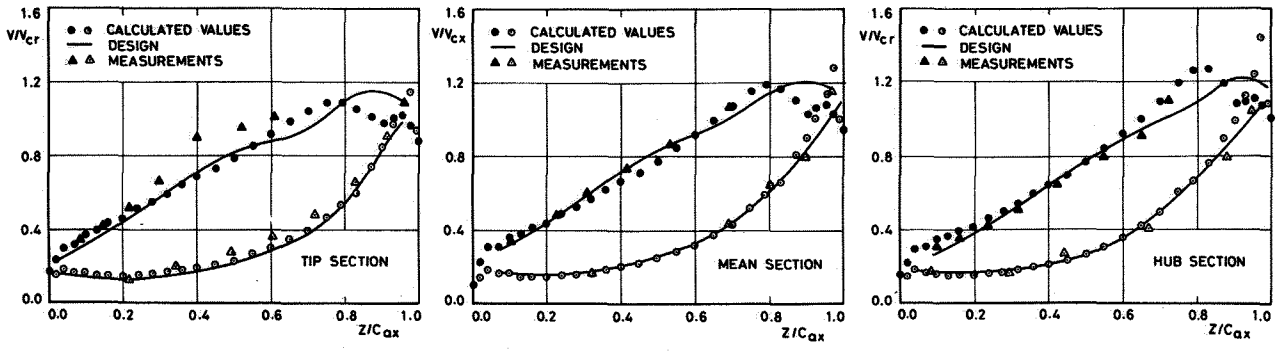

Fig. 15-Single stage axial turbine : stator blade velocity distributions

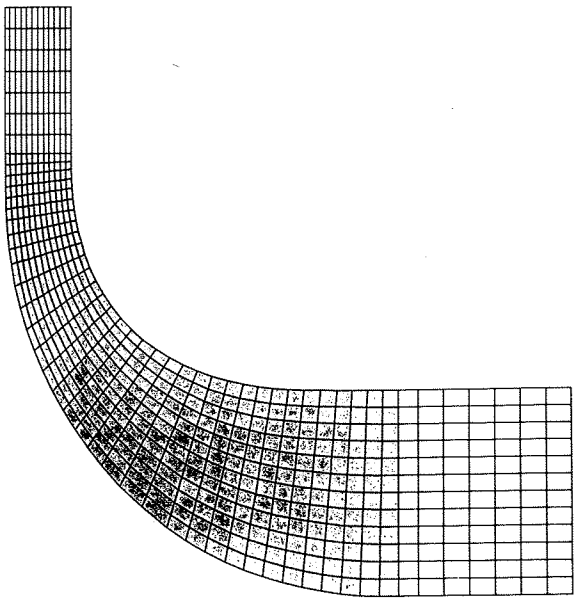

Fig. 16-Radial inflow turbine : computational domain

Geometry and measurements are described in [34] whereas computational results obtained by Choo & Civinskas from the 3D Denton's code are presented in [35]. For the present calculations, the computational domain (Fig. 16) was made of 49 spanwise surfaces (35 of them between leading and trailing edge), 13 bladewise surfaces (including suction and pressure surfaces) and 13 streamwise surfaces (including hub and tip). The inlet conditions to the rotor were uniform total pressure and temperature profiles, a uniform meridional flow angle profile (90° from axial) and a blade-to-blade flow angle profile as given in figure 17. The rotational speed was 31456 rev/min and the isentropic coefficient value was 1.4.

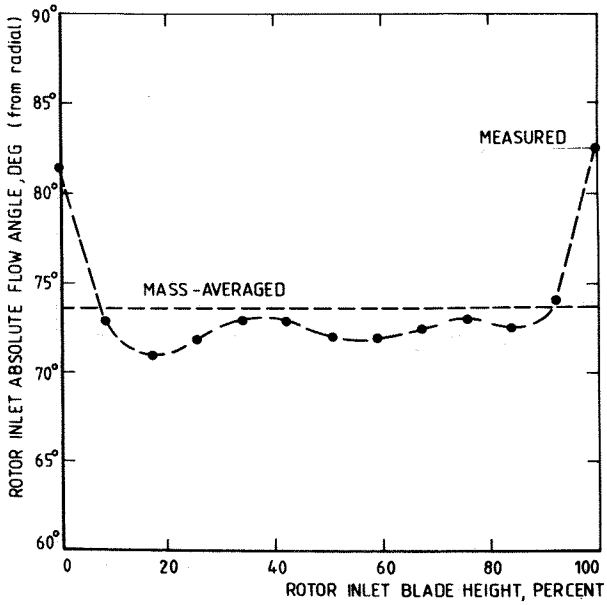

Fig. 17-Radial inflow turbine : blade-to-blade inlet angle profile

Two different calculations were performed. In the first one, a uniform (spanwise mass averaged) angle distribution was imposed in the inlet plane whereas the real, measured profile was used to perform the second computation (Fig. 17). The blade velocity distributions at hub and tip are shown in figure 18. The results obtained from the present method with the two different inlet angle distributions are compared to the results presented in [35].

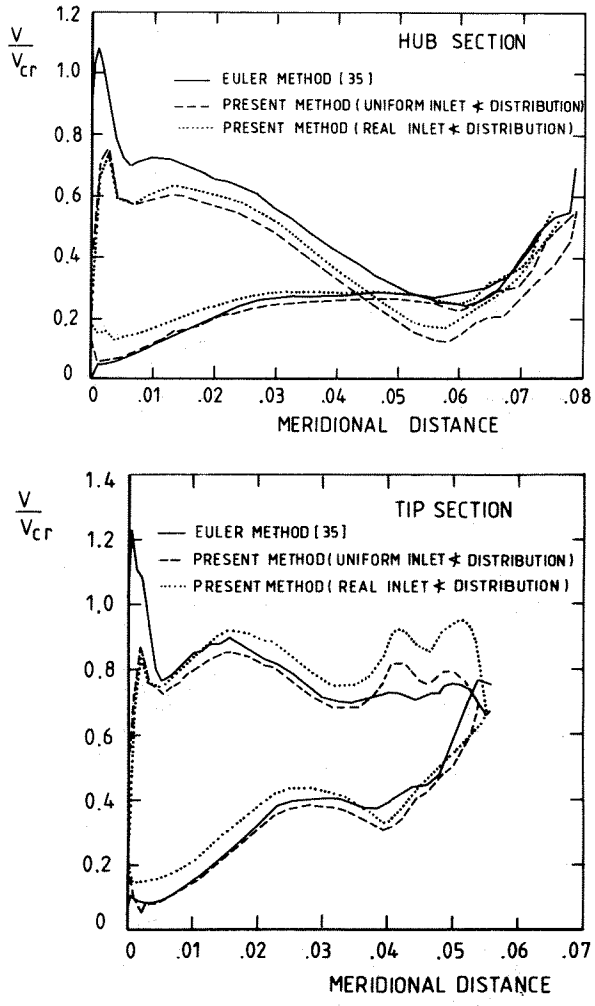

Fig. 18-Radial inflow turbine : blade velocity distribution

They are more or less in agreement along the major part of the blade, except in the leading edge region, where the results of Choo & Civinskas exhibit high pics in the front part of the suction side. The modeling of the rather thick leading edge might be responsible for these. Comparing the two results obtained from the present method allows the identification of small incidence effects. The computed and measured rotor exit flow angle distributions are compared in figure 19. The calculated flow angle were circumferentially mass averaged at the different heights of the channel. The use of the real inlet angle profile as upstream

boundary condition provides a better prediction of the turning. When using a uniform profile, the computed angles are obviously under-turned, especially in the hub region, with respect to the measurements. The calculated exit/inlet total pressure ratio distribution is compared to the measured one in figure 20. As should be expected, the present inviscid calculation predicts slightly higher values than the measured ones. This proves that the numerical diffusion, present in the computation, is maintained at low values, at least below the effect of physical viscosity on total pressure in the experiment.

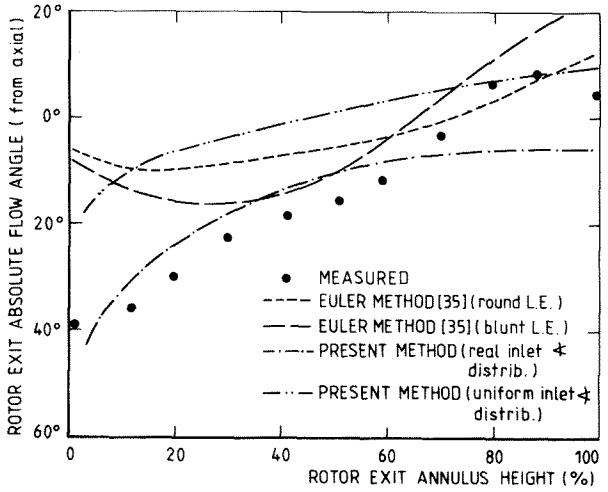

Fig. 19-Radial inflow turbine : outlet flow angle distribution

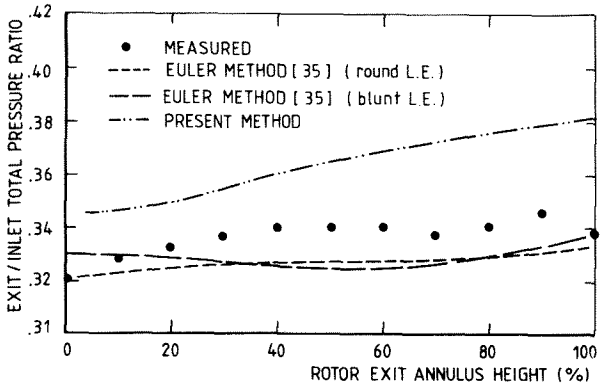

Fig. 20-Radial inflow turbine : outlet total pressure distribution

4.5 Radial compressor

The program has finally been applied to different radial compresor configurations without and with splitter blades. One of the classical test cases is the well known "Eckardt" backswept impeller [36], for which measurements and results from different computational programs (e.g. 3D Euler solvers and potential methods) are available. The drawbacks of this configuration for the validation of inviscid flow codes are the existence of separated flow and the limitation to a purely subsonic regime.

Geometry and measurements are described in [36]. Different computational results obtained from inviscid programs are presented in [37]. For the present calculation, the computational domain (Fig. 21) was made of 42 spanwise surfaces (29 of them between leading and trailing edge), 11 bladewise surfaces (including suction and pressure surfaces) and 11 streamwise surfaces (including hub and tip). The inlet conditions to the impeller were purely axial flow (in the blade-to-blade plane) and uniform total pressure and total temperature profiles. A slight contraction was applied at the exit of the vaneless diffuser to prevent possible exit flow instabilities. The rotational speed was 14000 rev/min and the isentropic coefficient value was fixed at 1.4. One of the numerical difficulties associated with this test case is the existence of extremely low velocities in the hub/pressure side corner. The results obtained from the present method did nevertheless reach a converged state according to the criteria defined in section 3.5.

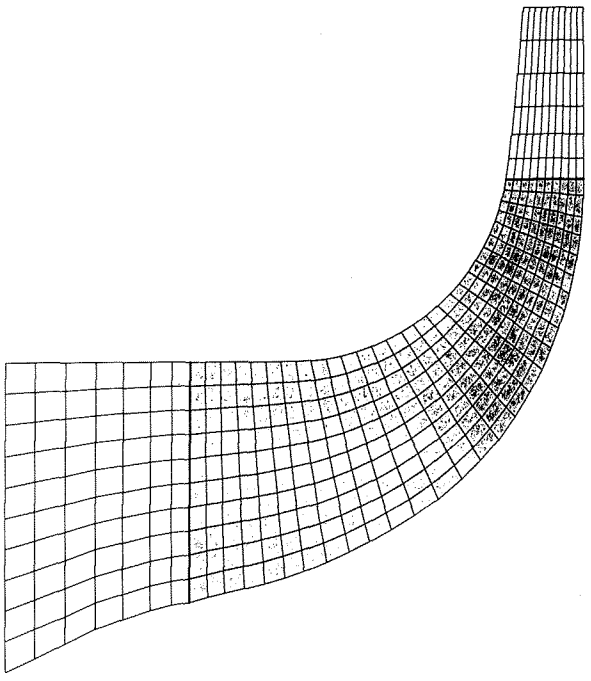

Fig. 21-Radial compressor : computational domain

Typical results are compared in figure 22 to solutions from alternative inviscid computational methods (Euler method [31] and potential method [7]). Along the hub section, the present method predicts a higher blade loading, principally because of the pressure side velocity distribution. Qualitative agreement exists with the potential method results along the suction side. Along the tip section, the present results also agree reasonably well with the

potential results, whereas the velocity distribution obtained from the other Euler code [31] is quite different. A possible explanation is that the authors of [37] mentioned that "they were not able to run the code to an asymptotic steady solution but had to stop the code were the solution appeared most satisfactory".

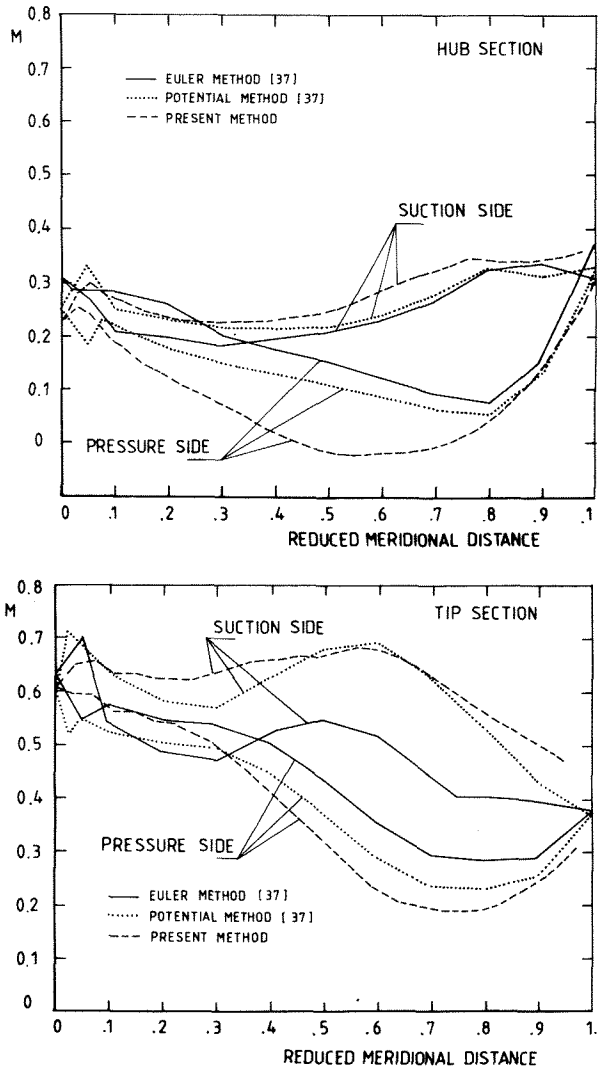

Fig. 22-Radial compressor : blade velocity distribution

5. SUMMARY-CONCLUSIONS

The application of a 3D Euler solver (finite volume discretization, time marching technique) to five different turbomachinery test cases has been presented. The obtained results agree generally well with experimental data, when available, and are most often supported by alternative numerical experiments. Although, because of space limitations, only few typical results have been presented, we hope to have demonstrated the generality and robustness of this approach with respect to

- the type of geometry (axial and radial components)
- the type of flow regime (subsonic and transonic)
- the type of configuration (isolated cascade or full "steady" stage).

REFERENCES

1. RIBAUT, M.: Three dimensional calculation of flow in turbomachines with the aid of singularities.
J.Engrg Power (ASME), Vol. 90, No 3, July 1968, pp 258-264.

2. MARTINON, J.: Use of the characteristic method for the prediction of the three dimensional flow field in high transonic compressors.
J.Engrg Power (ASME), Vol. 102, No 1, Jan 1980, pp 96-103.

3. DENTON, J.D.: A time marching method for two and three dimensional blade to blade flow.
ARC R&M 3775, 1975.

4. BOSMAN, C. & HIGHTON, J.: A calculation procedure for three dimensional time dependent, inviscid, compressible flow through turbomachinery blades of any geometry.
J.Mech.Engrg Sci., Vol. 21, No 1, 1979.

5. BROCHET, J.: Calcul numérique d'écoulements internes tridimensionnels transsoniques.
La Recherche Aérospatiale, No 5, 1980, pp 301-315.

6. THOMPKINS, W.T.: An experimental and computational study of flow in a transonic compressor rotor.
M.I.T., Ph.D. Thesis, June 1976.

7. LASKARIS, T.E.: Finite element analysis of three dimensional potential flow in turbomachines.
AIAA J., Vol. 16, No 7, July 1978.

8. SARATHY, K.P.: Computation of three dimensional flow fields through rotating blade rows and comparison with experiment.
J.Engrg Power (ASME), Vol. 104, No 2, April 1982, pp 394-402.

9. HOLMES, D.G. & TONG, S.S.: A three dimensional Euler solver for turbomachinery blade rows.
J.Engrg Gas Turbines & Power (ASME), Vol. 107, 1985, p. 258.

10. KOYA, M. & KOTAKE, S.: Numerical flow analysis of fully three dimensional turbine cascades.
J.Engrg Gas Turbines & Power (ASME), Vol. 107, 1985, p. 945.

11. McNALLY, W.D. & SOCKOL, P.M.: Computational methods for internal flows with emphasis on turbomachinery.
NASA TM 82 764, Nov. 1981.

12. VAN HOVE, W.: Calculation of three dimensional, inviscid, rotational flow in axial turbine blade rows.
J.Engrg Power (ASME), Vol. 106, No 2, April 1984, pp 430-436.

13. ARTS, T.: Etude de l'écoulement tridimensionnel dans un étage de turbine transsonique.
U. Catholique de Louvain, Ph.D. Thesis, 1982.

14. BOLETIS, E.; SIEVERDING, C.H.; VAN HOVE, W.: Effects of a skewed inlet endwall boundary layer on the three dimensional flow field in an annular turbine cascade.
AGARD CP 351, Paper 16, 1983.
15. ARTS, T.: Effects of tip endwall contouring on the three dimensional flow field in an annular turbine nozzle guide vane. Part 2 : Numerical investigation.
J.Engrg Gas Turbines & Power (ASME), Vol. 108, No 2, April 1986, pp 425-428.
16. ARTS, T.: Calculation of the three dimensional flow in the ultimate stator of a large steam turbine using a time marching method and a finite volume approach.
38th A.T.I. Congress, Bari, Italy, 1983.
17. ARTS, T.: Calculation of the three dimensional, steady, inviscid flow in a transonic axial turbine stage.
J.Engrg Gas Turbines & Power, Vol. 107, No 2, April 1985, pp 286-292.
18. ARTS, T.: Three dimensional rotational inviscid flow calculation in axial turbine blade rows.
von Karman Institute, TN 154, Sept. 1985.
19. ARTS, T.: On the consistency of four different control surfaces used for finite area blade to blade flow calculations.
IJ Num. Methods in Fluids, Vol. 4, No 11, Nov. 1984, pp 1083-1095.
20. McDONALD, P.W.: The computation of transonic flow through two dimensional gas turbine cascades.
ASME P 71 GT 89.
21. COUSTON, M.; McDONALD, P.W.; SMOLDEREN, J.J.: The damping surface technique for time dependent solutions to fluid dynamic problems.
von Karman Institute, TN 109, March 1975.
22. COUSTON, M.: Méthode de calcul de l'écoulement inter-aubes pseudo-tridimensionnel en régime transsonique.
U. Libre de Bruxelles, Ph.D. Thesis, 1976.
23. VAN HOVE, W. & ARTS, T.: Comparison of several finite difference schemes for time marching methods as applied to one dimensional nozzle flow.
von Karman Institute, TN 132, June 1979.
24. ARTS, T.: Cascade flow calculations using a finite volume method. in
von Karman Institute, LS 1982-07 "Numerical Methods for Flows in Turbomachinery Bladings".
25. LEHTHAUS, F.: Anwendung eines Zeit-Schritt-Verfahrens zur Berechnung der transsonischen Durchströmung ebener Turbinengitter und experimentelle Überprufung.
DFVLR 251 77 A 01, Feb. 1977.
26. Aero-Thermodynamics of Low Pressure Steam Turbines and Condensors.
von Karman Institute, LS 1983-06.
27. YOUNG, J.B.: Wet steam flow in LP turbines. in
von Karman Institute, LS 1983-06 "Aero-Thermodynamics of Low Pressure Steam Turbines and Condensers".
28. BOLETIS, E.: Effects of tip endwall contouring on the three dimensional flow field in an annular turbine nozzle guide vane. Part 1 - Experimental investigation.
J.Engrg Gas Turbines & Power, Vol. 107, No 4, Oct. 1985, pp 989-990.
29. ERDOS, J.I. & ALZNER, E.: Computation of unsteady transonic flows through rotating and stationary cascades.
NASA CR 2900, Dec. 1977.
30. MITCHELL, N.A.: A time marching method for unsteady two dimensional flow in a blade passage.
IJ Heat & Fluid Flow, Vol. 2, No 4, 1980, pp 205-220.
31. DENTON, J.D. & SINGH, U.K.: Time marching methods for turbomachinery calculations. in
von Karman Institute, LS 1979-07 "Application of Numerical Methods to Flow Calculations in Turbomachines".
32. SINGH, U.K.: A computation and comparison with measurements of transonic flow in an axial compressor stage with shock and boundary layer interaction.
J.Engrg Power (ASME), Vol. 104, No 4, April 1982, pp 510-515.
33. MOFFITT, T.P. et al.: Design and cold air test of single stage uncooled core turbine with high work output.
NASA TP 1680, June 1980.
34. McLALLIN, K.L. & HAAS, J.E.: Experimental performance and analysis of 15.04 centimeter tip diameter, radial inflow turbine with work factor of 1.126 and thick blading.
NASA TP 1730, 1980.
35. CHOO, Y.K. & CIVINSKAS, K.C.: Three dimensional inviscid analysis of radial turbine flow and a limited comparison with experimental data.
presented at ASME Annual Winter Meeting "Three Dimensional Flow Phenomena in Fluid Machinery", Miami, Nov. 1985.
36. ECKARDT, D.: Flow field analysis of radial and backswept centrifugal compressor impellers. Part I-Flow measurements using a laser velocimeter. in
Performance Prediction of Centrifugal Pumps and Compressors; Gopalakrishnan et al (eds), ASME 1980, pp 77-95.
37. PRINCE, T.C. & BRYANS, A.C.: Three dimensional inviscid computation of an impeller flow.
ASME P 83 GT 210.